

Novel BN Hollow Microspheres with Open Mouths – Facile Synthesis, Growth Mechanism, Resonant Raman Scattering Effect, and Cathodoluminescence Performance

Guangwu Wen,^{*[a,b]} Bo Zhong,^[a] Xiaoxiao Huang,^[a] Hongming Yu,^[a] Xiaodong Zhang,^[a] Tao Zhang,^[a] and Hongwei Bai^[a]

Keywords: Hollow microspheres / Boron nitride / Raman spectroscopy / Microreactors / Luminescence

Novel BN hollow microspheres have been successfully fabricated by a facile chemical vapour reaction approach using ammonia–borane as a precursor. The morphology and structure of the as-synthesized products are characterized by scanning electron microscopy (SEM), high-resolution transmission electron microscopy (HRTEM), selected-area electron diffraction (SAED), as well as electron energy loss spectroscopy (EELS). The hollow microspheres have open mouths and are 0.5–6 μm in diameter. The walls of the hollow spheres with thicknesses ranging from 200 to 800 nm are composed of poorly crystallized BN. The growth mechanism of the hollow microspheres is investigated and a growth

model is proposed. The BN hollow spheres show pronounced resonant Raman scattering character under illumination of a 457.9 nm laser line, which implies a potential photothermal effect. The hollow microspheres also exhibit intense cathodoluminescence emissions in the region of 200–400 nm, indicating that they could be potentially used as compact ultraviolet laser emitters. Moreover, the unique open-mouth feature, in combination with the superior thermal and chemical stability of BN, makes the BN hollow microspheres potential candidates as microreactors for investigations of high-temperature space-confined chemical reactions.

Introduction

Hollow micro/nanospheres are a new class of materials and have attracted immense interest in recent years owing to their unique properties and applications.^[1] For example, hollow spheres are conventionally used as fillers, pigments, coatings, and catalyst carriers due to their relatively low densities and high specific surface area.^[2] They also widely serve as vehicles for sheltering nanoparticles, proteins, enzymes, or DNA for drug delivery, diagnosis, and other biomedical applications.^[3] In addition, hollow spheres are also harnessed as ultra-small chemical reactors for the investigations of ultra-small-scale (10^{-9} – 10^{-18} L) chemical reactions.^[4] More recently, inspired by the fact that ultra-small-scale chemical reactions can be dramatically different from those at macro-scale due to space-confining effects,^[4b,5] there has been an increasing fascination with space-confined reactions, especially those occurring at high temperatures.^[6] In this regard, hollow spheres with open mouths, reliable chemical inertness, and, more importantly, excellent

thermal stability are highly desired and urgently needed. To date, a number of strategies have been reported on the fabrication of micro/nanospheres with hollow interiors, which include traditional template-assisted methods,^[7] self-templating approaches such as surface-protected etching,^[8] and chemical routes based on Ostwald ripening,^[9] the Kirkendall effect,^[10] and galvanic replacement.^[11] These methods have led to a rich variety of hollow microspheres, such as CuS,^[12] ZnO,^[13] CeO₂,^[14] and FeMoO₄.^[15] However, these successes are primarily limited to metals or metal compounds. The strategies listed above are mainly based on wet chemistry and thus are not applicable to fabricate hollow spheres of nonmetal covalent compounds which exhibit good thermal and chemical stability.

Hexagonal boron nitride (h-BN) is an analogue of graphite and has extensive applications in fields ranging from optical storage to medical treatment, photocatalysis, and electrical insulation due to its wide direct band gap (5.79 eV). It also has excellent chemical stability and resists oxidation.^[16] BN crucibles have been traditionally used as high-temperature reactors for many years owing to their excellent chemical inertness and thermal stability. Various BN micro/nanostructures have been successfully fabricated since the first discovery of BN nanotubes in 1995^[17] including nanowires,^[18] nanoplates,^[19] nanomeshes,^[20] conical nanorods,^[21] hollow nanoribbons,^[22] hollow nanocages,^[23] micro-/nanospheres,^[24] core-shell nanostructures,^[25] and

[a] School of Materials Science and Engineering, Harbin Institute of Technology, Harbin 150001, People's Republic of China
Fax: +86-451-8641-3922
E-mail: g.wen@hit.edu.cn

[b] School of Materials Science and Engineering, Harbin Institute of Technology (Weihai), Weihai 264209, People's Republic of China

Supporting information for this article is available on the WWW under <http://dx.doi.org/10.1002/ejic.201000703>.

few-atomic-layer sheets.^[26] However, to the best of our knowledge, investigations on the fabrication of BN hollow microspheres with open mouths have not been reported.

Herein, we report the synthesis of unique BN hollow microspheres with open mouths by a facile chemical vapor reaction approach employing ammonia–borane as a precursor. The morphology and structure of the BN hollow microspheres are characterized by means of complementary techniques. A possible growth mechanism of the hollow microspheres is proposed based on our experimental observations. The resonant Raman scattering character and cathodoluminescence (CL) performance of the hollow spheres have been investigated.

Results and Discussion

Morphology and Structure of the Products

Figure 1 presents the XRD pattern of the as-synthesized BN hollow spheres. All the diffraction peaks can be indexed to the hexagonal phase of BN with lattice parameters of $a = b = 2.504 \text{ \AA}$ and $c = 6.656 \text{ \AA}$ (JCPDS card No. 34-0421). No impurity phase was detected. It is worth noting that the diffraction peaks are markedly broadened, implying that the BN crystals in the hollow spheres have very small grain sizes. The morphology of the BN hollow spheres was examined by SEM. The low-magnification SEM images shown in Figure 2a–c demonstrate that the products are composed of a large number of microspheres. Figure 2d presents a high-magnification SEM image of the as-synthesized products, from which well-defined BN hollow microspheres with open mouths are clearly observed. Both the diameters and thicknesses of the BN hollow spheres have been statistically analyzed from the SEM images. The diameters of the microspheres exhibit a relatively wide distribution ranging from 0.5 to 6 μm with an average diameter of $3.4 \pm 1.3 \mu\text{m}$ (see statistical image inset in Figure 2b). The wall thicknesses of the microspheres are in the range of 200–800 nm (see statistical image in Figure S1). It is interesting to note that nearly all of the spheres are partially broken, which allows direct observation of the interior of the spheres and is also clear evidence of their hollow nature.

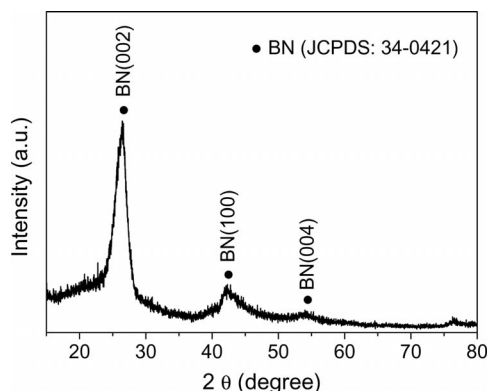


Figure 1. XRD pattern of the as-synthesized BN hollow spheres.

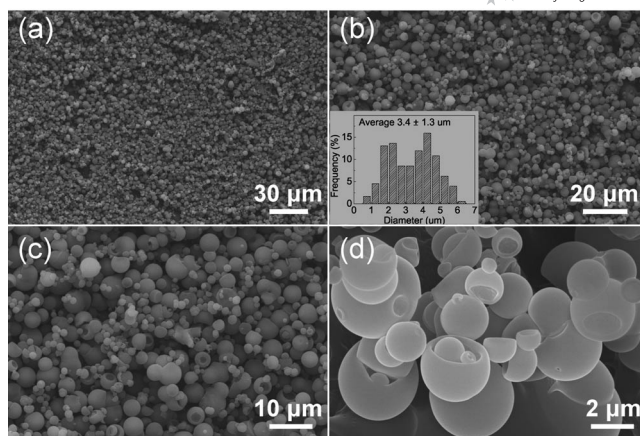


Figure 2. (a)–(c) Low- and (d) high-magnification SEM images of the BN hollow spheres. Inset: Statistical analysis of the diameters of the hollow spheres based on SEM images.

Figure 3a shows a TEM image of a typical BN hollow sphere, which additionally confirms the hollow nature of the microspheres. The selected-area electron diffraction (SAED) pattern of the hollow microsphere is displayed in the inset of Figure 3a. Two bright diffraction rings arising from the h-BN (100) and (110) planes are clearly observed, which indicates that the microspheres are composed of polycrystalline BN. However, the diffraction ring of the h-BN (002) planes is dramatically broadened, which indicates that the BN hollow spheres are poorly crystallized. To further characterize the structure of the hollow microspheres, HRTEM analysis was carried out. The magnified TEM image (Figure 3b) taken from the edge of the hollow microsphere, marked in Figure 3a, clearly shows that the wall thickness of the microsphere is about 50 nm. HRTEM images of the sphere wall displayed in Figure 3c,d additionally reveal that the crystallinity of the BN hollow sphere is poor.

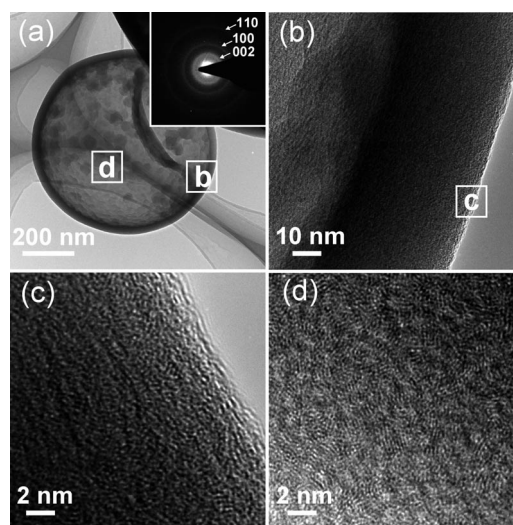


Figure 3. (a) TEM image of a typical BN hollow sphere. Inset: SAED pattern of the BN hollow sphere. (b)–(d) HRTEM images taken from the regions framed in (a) and (b).

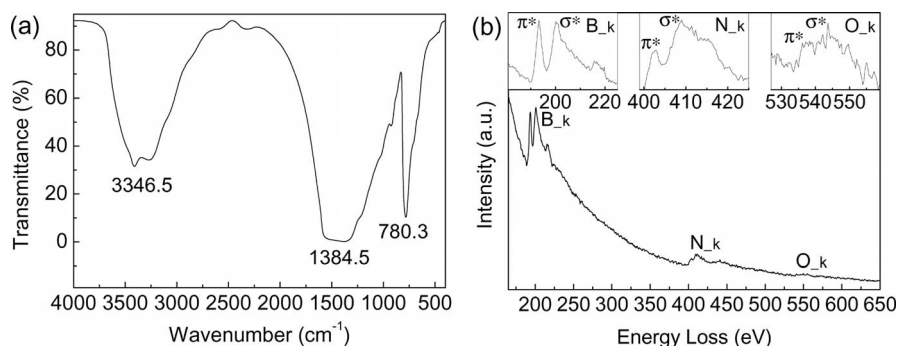


Figure 4. (a) FTIR and (b) EELS spectra of the BN hollow microspheres.

The BN hollow microspheres were analyzed by FTIR spectroscopy in transmittance mode to investigate the bonding nature, as shown in Figure 4a. Strong peaks centered at 1384.5 and 780.3 cm^{-1} are characteristic primary and secondary absorption bands of h-BN, indicating that the hollow microspheres are composed of h-BN. The broadening of the former peak is attributed to the B–O bond vibrations since these vibrations have many phonon modes in the 1500–1200 cm^{-1} range.^[27] The phonon mode at 3346.5 cm^{-1} is assigned to the O–H stretching mode. The presence of B–O and O–H bonds is ascribed to the moisture capture of the poorly crystallized h-BN from its surroundings.

EELS analysis was performed on the hollow microspheres to determine their chemical composition (Figure 4b). The pronounced peaks centred at around 188 and 401 eV in the EELS spectrum correspond to the characteristic *K*-shell ionization edges of B and N atoms, respectively.^[28] The sharp π^* and σ^* peaks identified from the spectrum are typical for the sp^2 bonding configuration, which is commonly observed in EELS spectra of h-BN.^[19] The 284 eV carbon *K* edge is notably absent, revealing that the microsphere is free of carbon. A small portion of oxygen was detected, and quasiquantitative analysis gives a B/N/O atomic ratio of 1:0.87:0.09.

Electron energy filtered TEM (EFTEM) analysis was conducted to track the compositional distribution within the BN hollow microspheres (Figure 5). Figure 5a shows the position where the mapping signals were collected. Figure 5b is a zero-energy-loss image showing the general morphology of a microsphere. Figure 5c–e shows B, N, and O elemental maps of the hollow microspheres, which were obtained with the energy loss windows centered at the boron *K* edge of 188 eV, the nitrogen *K* edge of 401 eV, and the oxygen *K* edge of 532 eV. These images intuitively suggest the presence of B, N, and O and that the elemental distributions are almost uniform throughout the sphere.

In agreement with the EELS results, XPS analysis additionally indicates that the as-obtained products contain B, N, and O, as evidenced by the wide-survey XPS spectrum shown in Figure 6. The carbon signal in the XPS profile is due to surface contamination during the exposure of the sample in the air before the examination. The broad B1s band can be decomposed into two Gaussian components

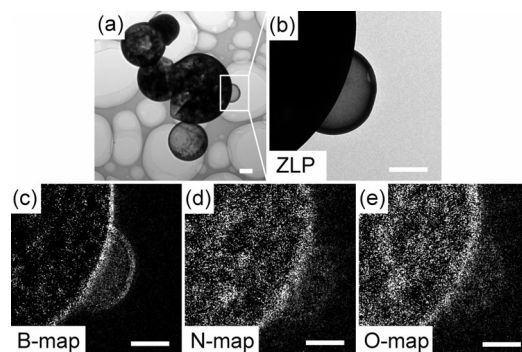


Figure 5. EFTEM analysis of the BN microspheres reflecting compositional distribution. (a) TEM image showing general morphology; (b) zero-loss image; (c)–(e) elemental maps (B, N, O). All scale bars represent 100 nm.

(inset upper left in Figure 6). The more intense component at 190.83 eV is assigned to boron atoms surrounded only by nitrogen atoms, similar to that in pure h-BN, whereas the component at 192.62 eV is attributed to boron atoms in a mixed oxygen/nitrogen environment, because the oxygen atoms are more electronegative than the nitrogen atoms and tend to cause the binding energy to shift upwards.^[29] The O1s spectrum, inset upper center in Figure 6, is of Gaussian type and is not decomposed further. The O1s peak centred at 532.87 eV is close to, but a little smaller than, the binding energy of O atoms in B_2O_3 (533.2 eV).^[30] This indicates that

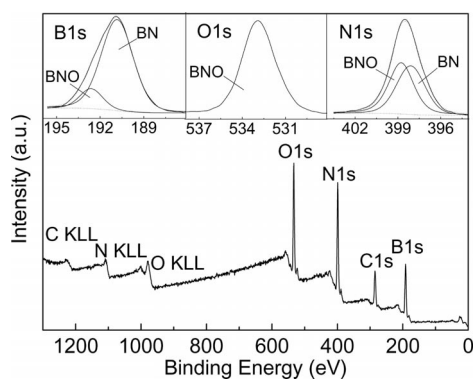


Figure 6. Wide scan, B1s (inset: upper left), O1s (inset: upper center) and N1s (inset: upper right) XPS spectra recorded from the BN hollow microspheres.

the O atoms not only bond with the B atoms, but also interact with the N atoms, as N atoms are less electronegative than O atoms and may cause the downward shift of the binding energy of O atoms. The N1s spectrum is presented in the inset upper right in Figure 6. One component at 398.10 eV can be associated with the presence of N–B bonds and the other component at 398.78 eV can be ascribed to oxynitrides.^[29]

It is worth noting that the presence of a small amount of oxygen appears to be inexplicable as we did not intentionally introduce any oxygen precursors during the sample fabrication, although the occurrence of trace oxygen is inevitable in high purity nitrogen. The trace oxygen is involved in the reaction, which results in oxygen in the BN microspheres. Moreover, it is well documented that h-BN (especially samples that are not well crystallized) tends to absorb moisture from its surroundings.^[31] Since these BN microspheres are poorly crystallized, the intrinsic moisture-absorption nature may also contribute to the oxygen in the BN microspheres.

Growth Mechanism

Based on our experimental observations, a growth model has been proposed to comprehend the formation process of the BN hollow microspheres. Figure 7a–f presents schematic illustrations and typical SEM images showing the different stages of the formation process. The growth process begins with the decomposition of the precursor ammonia–borane (AB). At elevated temperatures, AB decomposes according to the reaction $\text{H}_3\text{BNH}_3 \rightarrow \text{H}_2 + \text{BN}_x\text{H}_y$, where BN_xH_y indicates gaseous residues containing B and N atoms, including monomeric aminoborane (BH_2NH_2), borazine ($\text{B}_3\text{N}_3\text{H}_6$), and traces of diborane (B_2H_6).^[32] These gases could deposit on the bare graphite substrate and react with each other at appropriate temperatures resulting in a film (Figure 7a,b). Figure S2 presents a typical SEM image of the substrate obtained after pyrolysis, which clearly shows a thin film on the bare graphite substrate. The film is believed to be formed by the polymerization of gases decomposed from AB and is probably in a liquid state at high temperatures. During the polymerization of the B–N-containing film, hydrogen is released, and the film becomes more viscous. In this process, some hydrogen may be trapped in the viscous film, and when the hydrogen accumulation reaches the saturation point, the thin film may buckle (Figure 7c,d) and subsequently crack from the substrate, forming hollow microspheres and leaving holes on the substrate (Figure 7e,f). These assumptions are supported by our experimental observations. First, the diameters of the holes are around 3 μm and are comparable to that of the microspheres. This indicates that the hollow microspheres and the holes on the film are closely related and the hollow microspheres may be originally parts of the thin film on the substrate. Moreover, EDX analysis shows that the chemical compositions of the hollow BN spheres and that of the film are nearly identical (see Figure S3 in Supporting Information).

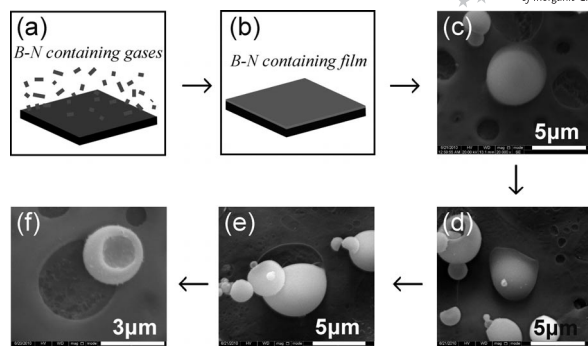


Figure 7. Schematic illustrations and representative SEM images showing the formation process of the BN microspheres: (a) initial bare graphite substrate; (b) formation of a thin film on the substrate; (c), (d) buckling of the thin film from the substrate due to hydrogen accumulation; (e), (f) cracking of the thin film to form BN hollow microspheres.

Another issue that should be clarified is that why the BN microspheres are not uniform. In our opinion, the size of the BN microspheres may be determined by the thickness of the B–N containing film. The thicker film possesses a higher strength and thus can trap more hydrogen before buckling and cracking than the thinner one. Therefore, the thicker film results in larger BN microspheres, whereas the thinner film results in smaller ones. This is supported by our SEM observations. Careful SEM examinations reveal that there is a positive relationship between the diameters and the wall thicknesses of the BN microspheres, i.e. larger microspheres always have thicker wall thicknesses and vice versa. The growth model proposed here is merely a phenomenological model. A detailed thermodynamic and kinetic model involving film formation, microsphere buckling, and cracking is required to give a complete and accurate description of the growth process of the BN microspheres and is currently underway.

Resonant Raman Scattering Effect

The Raman spectrum of the BN hollow microspheres, excited by using a 457.9 nm laser line, shows unanticipated features (Figure 8a, see also Figure S4 in the Supporting Information). The dominant peak at ca. 1367 cm^{-1} , which is normally observed for in-plane B–N vibrations (E_{2g} mode)^[33] in the Raman spectrum of h-BN is notably absent. Instead, we observed a series of periodic peaks with nearly uniform intervals. A Raman spectrum recorded from a different sample by using the same laser line shows a similar feature (see Figure 8b). The Raman spectra of the BN hollow microspheres exhibit multi-peaks at nearly equal intervals, but the intervals of the peaks are microsphere-dependent and are not necessarily the same for different spheres. These exceptional Raman scattering phenomena are tentatively explained within the framework of the resonant Raman scattering (RRS) theory.^[34] RRS occurs where the frequency of the incident radiation matches that of an electronic transition so that the selection rule for normal Ra-

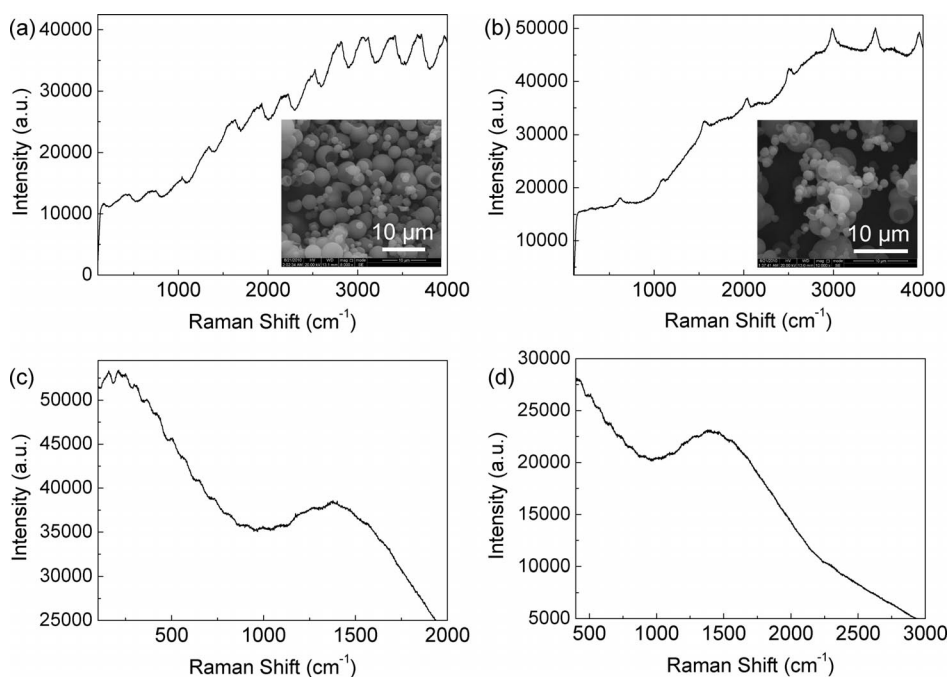


Figure 8. Representative Raman spectra of BN hollow microspheres recorded under different conditions: (a), (b) 457.9 nm laser line, 20 mW laser power, 5 s acquisition time, (c) 633 nm laser line, 10 mW laser power, 10 s acquisition time, and (d) 488 nm laser line, 20 mW laser power, 10 s acquisition time. Spectra (a), (c), and (d) are recorded from the same sample, whereas spectrum (b) is recorded from another sample to show the universality of the phenomenon. Insets: SEM images of corresponding samples.

man scattering is broken. Since there is no selection rule to forbid the overtones occurring, periodic multi-peaks are expected in resonant Raman spectra. Therefore, the nearly equally spaced peaks observed in our Raman spectra are believed to be the overtones of one vibration. It is worth noting that not all vibrations observed in conventional Raman spectra of h-BN are intensified by resonance,^[35] which accounts for the absence of the normal vibration mode at 1367 cm^{-1} . Another two laser lines (488 and 688 nm) were also used to irradiate the samples of the hollow microspheres, and the Raman spectra obtained are shown in Figure 8c,d. Overtones could also be identified in these spectra, but they are not as definite as in that irradiated by the 457.9 nm laser line. This means that lasers operating at 488 and 688 nm are not as effective as that at 457.9 nm in inducing RRS, probably because the condition for observing effective RRS is not satisfied by using 488 and 688 nm laser lines. It is generally accepted that the closer the excitation frequency of a laser beam is to that of an electron transition, the more effective the RRS.^[36] Therefore, the 457.9 nm laser line is closer to the frequency of an electron transition than the other two laser lines.

A crucial implication, which arises from the RRS effect of the BN hollow spheres, is that they possess a potential photothermal effect. In conventional Raman scattering analysis, spectroscopists prefer to avoid RRS, because when resonance conditions occur, the power of the laser is liable to adsorb into the sample. This may cause sample decomposition through photothermal effects or strong fluorescence.^[36,37] In our case, the photothermal effect of the RRS was utilized to heat the hollow microspheres. This heating

could facilitate the application of the BN hollow microspheres for the investigations of ultra-small-scale reactions since heating by laser could be well controlled in both time and space.

Cathodoluminescence Performance

Figure 9 displays a CL spectrum recorded from a typical hollow microsphere. Intense UV emission peaks in the region of 300–400 nm are clearly observed, indicating that the novel BN hollow microspheres could be potentially used as compact UV laser emitters. The broad luminescence bands at around 338.7 nm as well as the emission peaks located at

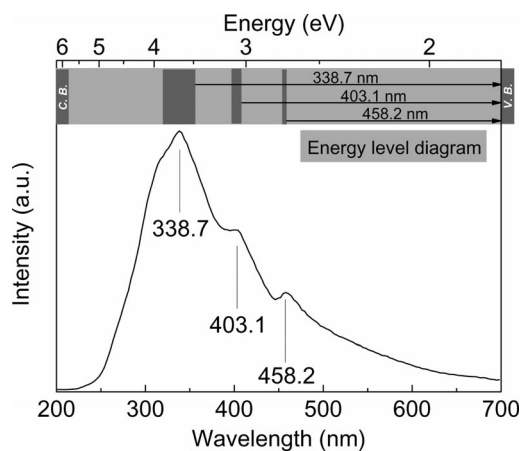


Figure 9. CL spectrum of the BN hollow microspheres. Inset: Schematic energy level diagram.

403.1 and 458.2 nm are assigned either to impurity (possibly oxygen) and defect centers or to radiative excitonic dark states. These bands are commonly observed in the luminescence spectra of multiwalled BN nanotubes, BN nanorods, and BN whiskers.^[38] An electron energy level diagram based on the CL spectrum was obtained, shown in the inset of Figure 9. It is worth noting that one of the energy levels (around 458.2 nm) is very close to the wavelength of the laser line (457.9 nm), which induces the maximum RRS. This means that the 457.9 nm laser used in the Raman analysis matches the true resonance frequency of an electron energy level so that the maximum RRS occurs. This further confirms that the peculiar Raman spectra exhibiting overtones are essentially caused by the RRS effect.

Conclusions

Novel BN hollow microspheres were successfully fabricated by a facile one-step approach employing ammonia-borane as a precursor. The hollow microspheres exhibit open mouths and have diameters ranging from 0.5 to 6 μm . The growth mechanism of the BN microspheres has been revealed based on our experimental findings, and the formation of a thin film containing B and N on the substrate is shown to be a crucial step in the growth process. The BN hollow microspheres exhibit an unexpected resonant Raman scattering effect under the illumination of a 457.9 nm laser line and show intense UV CL emissions in 200–400 nm wave bands. Such BN hollow microspheres may find application in the field of UV lasing and as small chemical reactors for the investigations of high-temperature space-confined reactions.

Experimental Section

Material Preparation: All the chemical reagents used in this study were of analytical grade (Shanghai Chemical Reagent Corp.). We prepared the BN hollow microspheres by a facile chemical vapor reaction route in a gas pressure furnace. Ammonia-borane (AB , $\text{H}_3\text{B}\cdot\text{NH}_3$) was used as a starting material. AB was synthesized according to the method proposed by Ramachandran et al.^[39] In a typical run, AB powder (3.0 g) was charged into an alumina crucible with a piece of graphite paper suspended in the center acting as a substrate. The crucible was subsequently mounted into the furnace chamber. The chamber was sealed and pumped to a base pressure of 0.1 Pa. High-purity nitrogen was introduced into the furnace chamber until a pressure of 0.5 MPa was reached. The furnace was heated to 900 $^\circ\text{C}$ at a rate of about 10 $^\circ\text{C}\text{min}^{-1}$ and kept at this temperature for 60 min before it was cooled to room temperature. White products resembling white coatings were obtained on the surface of the graphite paper and were directly used for characterization.

Characterization Techniques: The as-prepared samples were characterized by a variety of techniques including X-ray powder diffraction [XRD, Rigaku D/max- γB X-ray diffractometer with Cu- K radiation ($\lambda = 0.154178$ nm)], scanning electron microscopy [SEM, MX2600EF equipped with energy-dispersive X-ray spectroscopy (EDX)], conventional and high-resolution transmission electron microscopy [TEM and HRTEM, Philips Tecnai 20 and Tecnai F30

FEG equipped with electron energy loss spectroscopy (EELS), respectively], X-ray photoelectron spectroscopy [XPS, PHI 5700 ESCA System with a PC-ACCESS data analysis system (Physical Electronics Inc.)], and Fourier transformation infrared spectroscopy (FTIR, Perkin-Elmer spectrum one system by using pressed KBr disks). CL measurements were performed by using a Gatan MONOCL3+ system installed on a JSM-7000F FESEM. Raman spectra were recorded with a Jobin-Yvon HR800 spectrometer by using three laser lines (457.9, 488, and 633 nm) as excitation sources. The laser beams were focused to ca. 1 μm in diameter. The spectra were collected at ambient conditions.

Supporting Information (see footnote on the first page of this article): Statistical analysis of the wall thickness of the BN hollow spheres; SEM image showing a thin layer was formed on the substrate; EDX spectra of the hollow microspheres and the layer deposited on the substrate; additional Raman spectra of the BN hollow microspheres obtained using a 457.9 nm laser line.

Acknowledgments

This work was supported by the National High-tech R&D Program (863 Program) (No. 2007AA03Z340), the National Science Foundation of China (No. 50672018), and the Program of Excellent Team in Harbin Institute of Technology.

- [1] a) Q. Zhang, W. Wang, J. Goebel, Y. Yin, *Nano Today* **2009**, *4*, 494–507; b) H. P. Cong, S. H. Yu, *Adv. Funct. Mater.* **2007**, *17*, 1814–1820.
- [2] a) M. Ohmori, E. Matijevic, *J. Colloid Interface Sci.* **1992**, *150*, 594–598; b) W. W. Wang, Y. J. Zhu, L. X. Yang, *Adv. Funct. Mater.* **2007**, *17*, 59–64; c) J. K. Yuan, K. Laubernds, Q. H. Zhang, S. L. Suib, *J. Am. Chem. Soc.* **2003**, *125*, 4966–4967.
- [3] a) W. M. Zhang, J. S. Hu, Y. G. Guo, S. F. Zheng, L. S. Zhong, W. G. Song, L. J. Wan, *Adv. Mater.* **2008**, *20*, 1160–1165; b) Y. F. Zhu, J. L. Shi, W. H. Shen, X. P. Dong, J. W. Feng, M. L. Ruan, Y. S. Li, *Angew. Chem. Int. Ed.* **2005**, *44*, 5083–5087; c) P. R. Leduc, M. S. Wong, P. M. Ferreira, R. E. Groff, K. Haslinger, M. P. Koonce, W. Y. Lee, J. C. Love, J. A. McCammon, N. A. Monteiro-Riviere, V. M. Rotello, G. W. Rubloff, R. Westervelt, M. Yoda, *Nat. Nanotechnol.* **2007**, *2*, 3–7.
- [4] a) A. Dudia, A. Kocer, V. Subramaniam, J. S. Kanger, *Nano Lett.* **2008**, *8*, 1105–1110; b) T. Shimizu, *J. Polym. Sci. Pol. Chem.* **2008**, *46*, 2601–2611.
- [5] a) Q. H. Yang, D. F. Han, H. Q. Yang, C. Li, *Chem. Asian J.* **2008**, *3*, 1214–1229; b) P. Anzenbacher, M. A. Palacios, *Nat. Chem.* **2009**, *1*, 80–86.
- [6] G. Dmitri, B. Yoshio, M. Masanori, F. Keita, T. Chengchun, *Acta Mater.* **2004**, *52*, 3295–3303.
- [7] J. G. Wang, Q. Xiao, H. J. Zhou, P. C. Sun, Z. Y. Yuan, B. H. Li, D. T. Ding, A. C. Shi, T. H. Chen, *Adv. Mater.* **2006**, *18*, 3284–3288.
- [8] Q. Zhang, T. R. Zhang, J. P. Ge, Y. D. Yin, *Nano Lett.* **2008**, *8*, 2867–2871.
- [9] W. S. Wang, L. Zhen, C. Y. Xu, W. Z. Shao, *J. Phys. Chem. C* **2008**, *112*, 14360–14366.
- [10] H. C. Zeng, *J. Mater. Chem.* **2006**, *16*, 649–662.
- [11] Y. G. Sun, B. T. Mayers, Y. N. Xia, *Nano Lett.* **2002**, *2*, 481–485.
- [12] L. Ge, X. Y. Jing, J. Wang, S. Jamil, Q. Liu, D. L. Song, J. Wang, Y. Xie, P. P. Yang, M. L. Zhang, *Cryst. Growth Des.* **2010**, *10*, 1688–1692.
- [13] Y. C. Qiu, W. Chen, S. H. Yang, B. Zhang, X. X. Zhang, Y. C. Zhong, K. S. Wong, *Cryst. Growth Des.* **2010**, *10*, 177–183.
- [14] Z. J. Yang, D. Q. Han, D. L. Ma, H. Liang, L. Liu, Y. Z. Yang, *Cryst. Growth Des.* **2010**, *10*, 291–295.
- [15] L. Zhang, X. F. Cao, Y. L. Ma, X. T. Chen, Z. L. Xue, *Crystengcomm* **2010**, *12*, 207–210.

- [16] a) K. Watanabe, T. Taniguchi, H. Kanda, *Nat. Mater.* **2004**, *3*, 404–409; b) Y. Kubota, K. Watanabe, O. Tsuda, T. Taniguchi, *Science* **2007**, *317*, 932–934.
- [17] N. G. Chopra, R. J. Luyken, K. Cherrey, V. H. Crespi, M. L. Cohen, S. G. Louie, A. Zettl, *Science* **1995**, *269*, 966–967.
- [18] K. F. Huo, Z. Hu, F. Chen, J. J. Fu, Y. Chen, B. H. Liu, J. Ding, Z. L. Dong, T. White, *Appl. Phys. Lett.* **2002**, *80*, 3611–3613.
- [19] L. Q. Xu, J. H. Zhan, J. Q. Hu, Y. Bando, X. L. Yuan, T. Sekiguchi, M. Mitome, D. Golberg, *Adv. Mater.* **2007**, *19*, 2141–2144.
- [20] M. Corso, W. Auwarter, M. Muntwiler, A. Tamai, T. Greber, J. Osterwalder, *Science* **2004**, *303*, 217–220.
- [21] H. Z. Zhang, M. R. Phillips, J. D. Fitzgerald, J. Yu, Y. Chen, *Appl. Phys. Lett.* **2006**, *88*, 0931171–0931173.
- [22] Z. G. Chen, J. Zou, G. Liu, F. Li, Y. Wang, L. Z. Wang, X. L. Yuan, T. Sekiguchi, H. M. Cheng, G. Q. Lu, *Acs Nano* **2008**, *2*, 2183–2191.
- [23] a) W. S. Zhang, J. G. Zheng, W. F. Li, D. Y. Geng, Z. D. Zhang, *J. Nanomater.* **2009**, 264026; b) Y. Pan, K. F. Huo, Y. M. Hu, J. J. Fu, Y. N. Lu, Z. D. Dai, Z. Hu, Y. Chen, *Small* **2005**, *1*, 1199–1203.
- [24] a) Y. T. Wang, Y. Yamamoto, H. Kiyono, S. Shimada, *J. Am. Ceram. Soc.* **2009**, *92*, 787–792; b) L. Y. Chen, Y. L. Gu, L. Shi, Z. H. Yang, J. H. Ma, Y. T. Qian, *Solid State Commun.* **2004**, *130*, 537–540; c) T. Zhang, G. Wen, L. Xia, X. X. Huang, B. Zhong, X. D. Zhang, H. W. Bai, H. M. Yu, *Scripta Mater.* **2010**, *63*, 415–417.
- [25] Y. Zhang, K. Suenaga, C. Colliex, S. Iijima, *Science* **1998**, *281*, 973–975.
- [26] D. Pacile, J. C. Meyer, C. O. Girit, A. Zettl, *Appl. Phys. Lett.* **2008**, *92*, 1331071–1331073.
- [27] T. Matsuda, *J. Mater. Sci.* **1988**, *24*, 2353–2357.
- [28] Z. G. Chen, J. Zou, F. Li, G. Liu, D. M. Tang, D. Li, C. Liu, X. L. Ma, H. M. Cheng, G. Q. Lu, Z. D. Zhang, *Adv. Funct. Mater.* **2007**, *17*, 3371–3376.
- [29] C. Guimon, D. Gonbeau, G. Pfister-Guillouzo, O. Dugne, A. Guette, R. Naslain, M. Lahaye, *Surf. Interface Anal.* **1990**, *16*, 440–445.
- [30] D. J. Joyner, D. M. Hercules, *J. Chem. Phys.* **1980**, *72*, 1095–1108.
- [31] C. G. Cofer, J. Economy, *Carbon* **1995**, *33*, 389–395.
- [32] F. Baitalow, J. Baumann, G. Wolf, K. Jaenicke-Rossler, G. Leitner, *Thermochim. Acta* **2002**, *391*, 159–168.
- [33] C. H. Lee, J. S. Wang, V. K. Kayatsha, J. Y. Huang, Y. K. Yap, *Nanotechnology* **2008**, *19*, 455605.
- [34] R. J. H. Clark, T. J. Dines, *Angew. Chem. Int. Ed. Engl.* **1986**, *25*, 131–158.
- [35] E. V. Efremov, F. Ariese, A. J. G. Mank, C. Gooijert, *Anal. Chem.* **2006**, *78*, 3152–3157.
- [36] E. Smith, G. Dent, *Modern Raman Spectroscopy: A Practical Approach*, John Wiley & Sons, Chichester, **2005**.
- [37] K. A. Alim, V. A. Fonoberov, A. A. Balandin, *Appl. Phys. Lett.* **2005**, *86*, 053103.
- [38] a) C. C. Tang, Y. Bando, C. Y. Zhi, D. Golberg, *Chem. Commun.* **2007**, 4599–4601; b) C. Y. Su, W. Y. Chu, Z. Y. Juang, K. F. Chen, B. M. Cheng, F. R. Chen, K. C. Leou, C. H. Tsai, *J. Phys. Chem. C* **2009**, *113*, 14732–14738.
- [39] P. V. Ramachandran, P. D. Gagare, *Inorg. Chem.* **2007**, *46*, 7810–7817.

Received: June 28, 2010

Published Online: October 29, 2010